

1 Brief communication - Vent opening at Campi Flegrei: clues from 2 dyke propagation patterns

3 Jacopo Selva¹, Nello Mangone¹

4 ¹Dipartimento di Scienze della Terra, dell'Ambiente e delle Risorse (DiSTAR), University of Naples Federico II, Naples Italy
5 *Correspondence to:* Jacopo Selva (jacopo.selva@unina.it)

6 **Abstract.** Forecasting future vent opening position is fundamental for managing volcanic hazards, and is usually based on
7 the spatial density of past vents or other crust weakness indicators. Here, a novel empirical approach inspired by dyke
8 propagation models is applied to the Campi Flegrei caldera. Results show that dyke azimuthal direction and propagation
9 length are statistically independent, that azimuth correlates with topographic peaks within 7 km from the caldera centre, and
10 that propagation length exhibits two main peaks at 2 and 4 km. Based on these results, we develop two new vent opening
11 probability maps with maxima well correlating with caldera's structure and recent major seismicity.

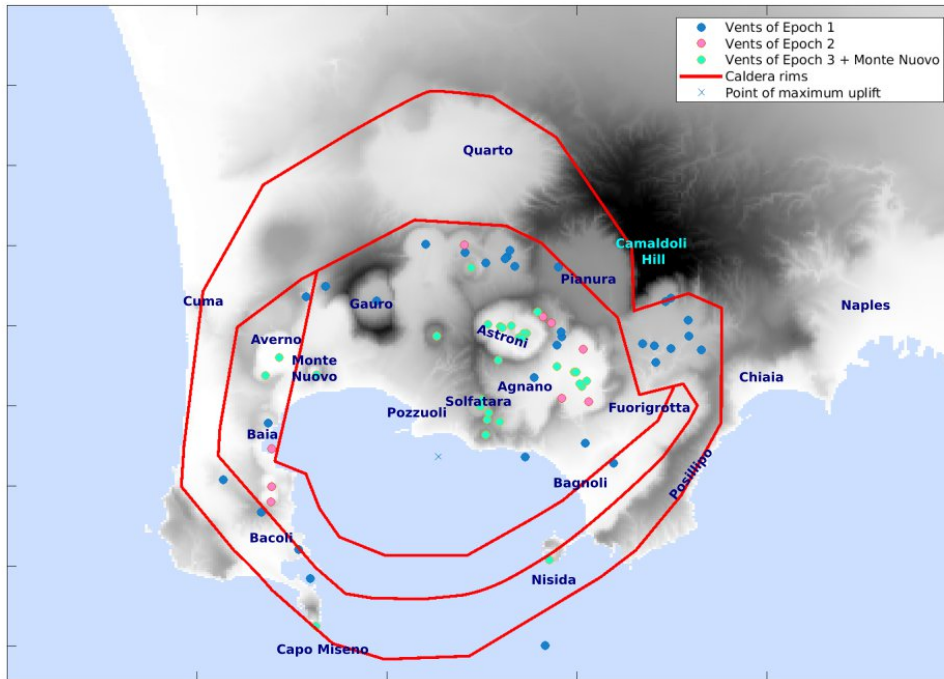
12 1 Introduction

13 The Campi Flegrei caldera volcanic activity dates back to the upper Pleistocene, with the earliest volcanic activity observed
14 in outcrops estimated at approximately 80 kyr (Pappalardo et al. 1999; Scarpati et al. 2013). Recent studies identified
15 widespread tephra layers originated from Campi Flegrei, extending its activity to nearly 200 kyr (e.g., Monaco et al., 2022;
16 Fernandez et al., 2024; Sparice et al., 2024). The first caldera collapse occurred approximately 39,000 years ago with the
17 Campanian Ignimbrite (CI) eruption (Giaccio et al. 2017). A second major eruption occurred around 14,000 years ago, the
18 Neapolitan Yellow Tuff (NYT), possibly causing a second collapse, after which volcanic activity resumed within the caldera
19 (Orsi et al. 2004).

20 The post-NYT eruptive history is divided into three main epochs (Di Vito et al. 1999, Bevilacqua et al. 2016, Fig. 1). The
21 first epoch comprises at least 33 eruptions, spanning from 14,000 to 10,600 years ago. The eruptive vents align with the
22 caldera boundaries, with the most energetic eruption being that of the "Pomici Principali" around 12,000 years ago
23 (Bevilacqua et al. 2016). The second epoch follows a relatively brief quiescent period and includes nine eruptions dated
24 between 9,600 and 9,100 years ago, primarily concentrated in the northeastern sector of the caldera. The third epoch
25 encompasses a total of 26 eruptions from approximately 5,500 to 3,800 years ago. Its activity was predominantly focused in
26 the northeastern part of the caldera (Agnano area), secondarily in the northwestern sector (Averno area), and concluded with
27 peripheral distal eruptions (Nisida, Capo Miseno, and Fossa Lupara (Natale et al., 2025). The most energetic eruption during
28 this period was that of Agnano-Monte Spina around 4,500 years ago (Bevilacqua et al. 2016). The long period of quiescence
29 following the third epoch lasted until 1538 AD, when the Monte Nuovo eruption took place in the northwestern sector of the
30 caldera (Di Vito et al., 2016). The caldera has not experienced any eruption since.

31 After NYT, the caldera experienced significant resurgence, accompanied by seismicity, degassing, and slow ground
32 deformation often referred to as bradyseism (Isaia et al., 2019; Natale et al., 2022). The latter is centred mainly in the
33 Pozzuoli area, which is approximately at the centre of the caldera (Fig. 1), and major movements were tracked at least from
34 the 4th century AD thanks to the ruins of a Roman temple in the port of this city, known as the Serapeum (Di Vito et al.
35 2016; Natale et al. 2023). The largest known bradyseismic events are the ones related to the last Campi Flegrei eruption (the
36 1538 Monte Nuovo eruption, Di Vito et al., 2016). In the last century, three main bradyseismic crises occurred in 1950-52,
37 1970-72, and 1982-84, characterised by episodes of uplift of more than 1 m interrupting a slow long-lasting subsidence (Del
38 Gaudio et al 2010). Approximately in 2005, a slow uplift started, accelerating over time, which fully recovered the

39 subsidence in 2021, and now exceeds the uplift peaks observed in the last century (Bevilacqua et al. 2024). This event is still
40 ongoing.



41
42 **Figure 1:** Toponymic map of the Campi Flegrei caldera, along with the vent positions of post-NYT eruptions (from Bevilacqua et al.
43 2016) and the caldera rims (Natale et al. 2024, 2025). For simplicity, Monte Nuovo is included in Epoch 3.
44
45

46 Forecasting vent opening is crucial for any volcanic hazard quantification, especially in calderas. Different approaches were
47 adopted at Campi Flegrei through time. Alberico et al. (2002) developed a method identifying crustal weaknesses using
48 geophysical, geological, and geochemical parameters. Their probability map indicates the highest likelihood of vent
49 openings in the central caldera near Pozzuoli (Fig. 1). Selva et al. (2012) utilized a Bayesian approach fed by fewer
50 parameters, focusing on tectonic structures recognized at that time, to track crust weakness, and past vents, shifting the area
51 at higher probability toward the northeastern and northwestern sectors, where post-NYT activity concentrated. Bevilacqua et
52 al. (2015) adopted a method based on Gaussian kernel and accounting for the uncertainty on past vent positions, confirming
53 the northeastern sector (near Agnano and Astroni, Fig. 1) as the most likely area for future eruptions. Both Selva et al. (2012)
54 and Bevilacqua et al. (2015) included also a formal quantification of the epistemic uncertainty in their models, accounting
55 for model uncertainty. More recently, based on past observations and removing multiple eruptions from clustered vents,
56 Charlton et al. (2020) noted that vent opening occurred substantially randomly within a ring area surrounding the caldera
57 centre, corresponding to the caldera rim (Fig. 1), producing a new qualitative indication about potential future vent opening.
58 Rivalta et al. (2019) studied the physical propagation of magma dykes by modelling the trajectory of potential dykes due to
59 the subsurface stress field and the dike's initial position. Their model accounts for various stresses affecting magma ascent.
60 For calderas, it suggests that eruptive vents are concentrated at specific distances from the centre, influenced by the stress
61 induced by the caldera depression, defining a higher propensity to eruption closer to caldera rims, as noted by Charlton et al.
62 (2020). Considering the caldera depression size, Rivalta et al. (2019) forecasted for Campi Flegrei a potential peak for vent
63 opening at a semi-annular belt located between 2.3 and 4.2 km from the caldera centre. Rivalta et al. (2019) analysed the
64 effect of caldera unloading, as well as those of topographic peaks, which may break the caldera symmetry. They analysed the
65 case of the Campi Flegrei caldera, explaining the concentration of volcanic activity in the northeastern sector due to the peak
66 of the Camaldoli Hill (Fig. 1), which creates a stress field that may favour magma trajectories in the north-east direction.

67 The main features of Rivalta et al. (2019) model are i) that the geometry of the caldera (unloading effect) significantly
68 influences dykes propagation outward, promoting eruptions away from the geometric centre of the caldera, and ii)
69 topographic asymmetries create localised stress variations in the subsurface, affecting eruption frequency across different
70 angular sectors. While a sufficiently detailed knowledge of the sub-surface stress state is difficult to reach, it is possible to
71 verify if these two main features left a trace on the available record of past vent positions, and to use this empirical signature
72 to define new vent opening probability maps.

73 2 Method

74 Rivalta et al. (2019) found that the path of the dykes feeding eruptions is mainly controlled by the geometry of the caldera,
75 which determines the distance from the centre of the caldera, and by the topographical peaks surrounding the caldera, which
76 establishes preferential directions for propagation. To this end, Rivalta et al. (2019) assumed that the origin at depth of the
77 magma is located at the centre of the caldera, 3 km below the location of the maximum observed uplift (Amoruso et al. 2014,
78 Rivalta et al. 2019, Buono et al. 2025), and producing mostly lateral propagation with trajectories controlled by the structure
79 of the caldera and the consequent stress field.

80 Assuming a magma origin located around the centre of the caldera, independently of its specific depth and geometry, the
81 empirical track of these features may be retrieved by studying the distribution of past vents around the caldera centre. These
82 empirical distributions can then be used to set a vent opening probability map. The probability density function in a specific
83 point in the caldera can be calculated in polar coordinates using the following formula:

$$84 \quad f_{pol}(r, \theta) = f_r(r) f_\theta(\theta). \quad (1)$$

85 where the term $f_r(r)$ is the probability distribution for the distances from the centre of the caldera and the term $f_\theta(\theta)$ is the
86 angular probability distribution. In this formulation, it is assumed that these two distributions can be considered independent.
87 Indeed, the physical process described in Rivalta et al. (2019) suggests a potential independence between direction of dyke
88 propagation and distance from the caldera centre, as they are controlled by two different features of the caldera, being the
89 distance fundamentally controlled by the size of the nearly circular shape of the caldera, and the direction predominantly
90 controlled by local topographic features. This independence should also leave an empirical track in past vent positions,
91 which can also be formally verified by testing whether the direction and the distances found using past vent positions are
92 correlated to each other.

93 The probability distribution of eq. (1) can be transformed into Cartesian coordinates as follows:

$$94 \quad f_{xy}(x, y) = \frac{1}{r} f_{pol}(r, \theta) = \frac{1}{r} f_r(r) f_\theta(\theta) \quad (2)$$

95 where the term $f_{pol}(r, \theta)$ is again factorized in its two terms using Eq. (1). Defining an application grid, equation (2) can be
96 used to establish a vent probability map by substituting $f_r(r)$ and $f_\theta(\theta)$ with the appropriate distributions of potential distance-
97 from-centre and azimuth. Depending on the available data, such distributions may be estimated empirically, looking at the
98 distribution of past vents, including all the data that reflect the present state the caldera, or analysing the topographical peaks
99 surrounding the caldera.

100 3. Results

101 The position of the caldera centre is here assumed at the point of maximum uplift, here set 800 meters south of the GNSS
102 station of Rite at coordinates LON 426355 and LAT 4518743 (UTM WGS84, zone 33N; Bevilacqua et al., 2024, Fig. 1).
103 To establish an empirical model, we study the empirical distribution of azimuth (angle to the North of the line connecting the
104 centre of the caldera and the vent, hereinafter angle or azimuth) and distance-from-the-centre of the caldera (hereinafter
105 distance) of past eruptions. We consider the 71 vent positions of the post-NYT activity (Bevilacqua et al. 2016). Past vent
106 positions are affected by significant uncertainty. To evaluate their potential impact all statistical analyses, we consider the
107 uncertainty bounds defined in Bevilacqua et al. (2016), accounting for the uncertainty by randomly sampling 1000
108 alternative synthetic positions uniformly distributed within the defined uncertainty bounds (Supplementary Figure 1).

109

110 3.1 Empirical distributions of distance and azimuth

111

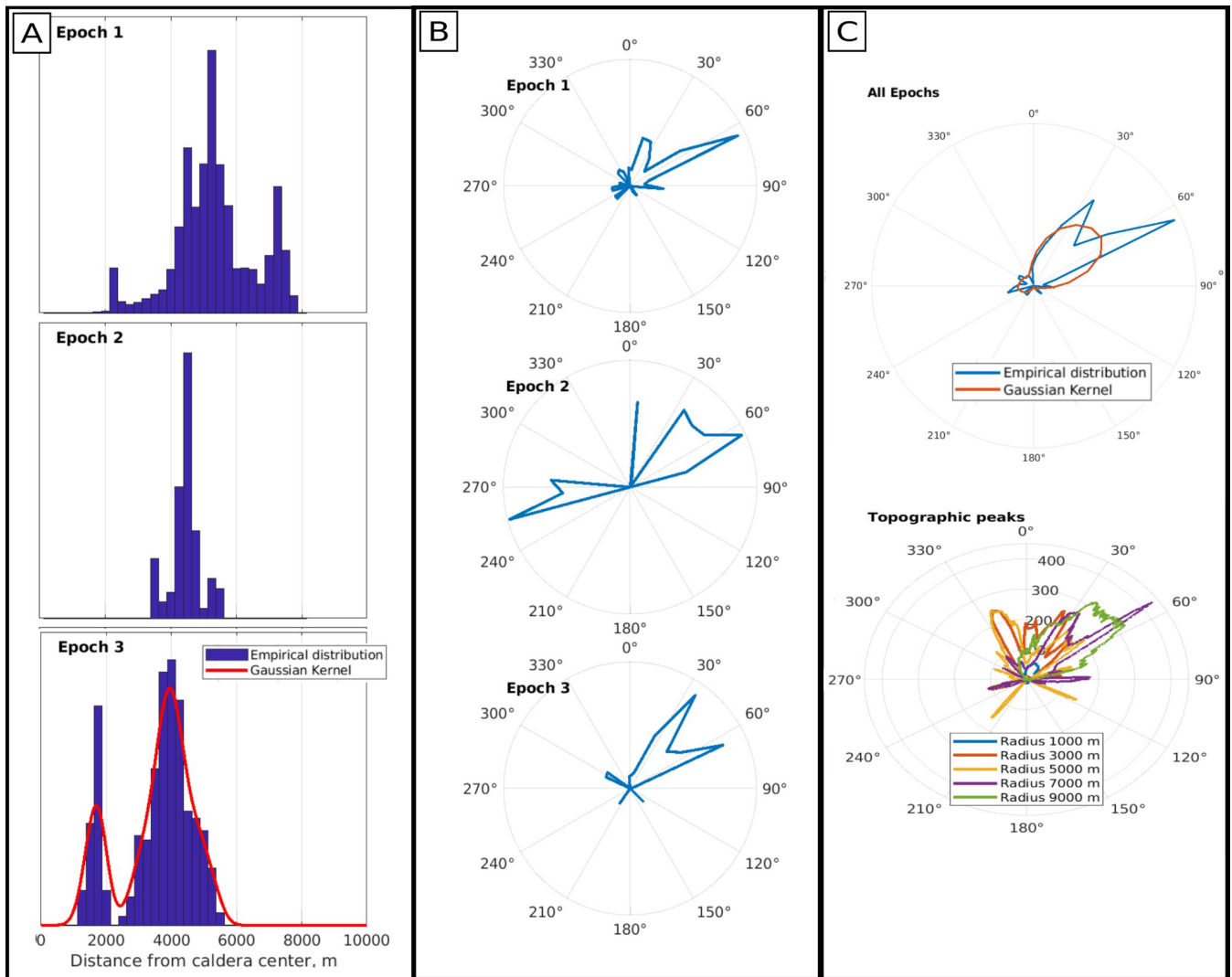
112 We first analyse the distances between the centre of the caldera and all post-NYT vents. Under the assumption of
113 propagation from the caldera centre, this distance represents the length of the horizontal propagation of the dykes that
114 alimented such eruptions. The analysis is conducted separately for the three epochs. For simplicity, the recent Monte Nuovo
115 eruption is included in the third epoch. In Figure 2A, we report the empirical distributions (histograms with bins of 250 m,
116 the corresponding empirical cumulative distribution functions are reported in Supplementary Figure 2), revealing a strong
117 difference between the first epoch, where 60% of eruptions occur between 4,400 and 6,600 m, and the third epoch that shows
118 shorter distances, with two significant peaks around 4,000 m and 2,000 m, being Epoch 2 somehow intermediate between the
119 other two.

120 To test if the distributions for the different Epochs are different, we implement a two-sample Kolmogorov-Smirnov test
121 (KS2), a non-parametric statistical test used to determine if two independent datasets are drawn from the same underlying
122 distribution (Gibbons and Chakraborti, 2003). Here and in the following tests, the significance level (red line) is set to 0.01
123 and it is corrected for multiple testing using the Bonferroni (1936) criterion, which consists of dividing the significance level
124 by the number of comparisons. The test confirms that the difference between Epoch 1 and Epoch 3 is statistically significant
125 also accounting for vent position uncertainty (see Supplementary Figure 3), confirming the already observed progressive
126 inward migration of post-NYT volcanism (Rivalta et al. 2019).

127 Following Rivalta et al. (2019), under the assumption of propagation from the caldera centre, the direction of propagation of
128 the dykes is controlled by topographic asymmetries. This direction can be investigated by analysing the azimuth of past
129 vents with respect to the centre of the caldera. In Figure 2B, we report the empirical distributions for the different epochs
130 (histogram with bins of 20 degrees, the corresponding empirical cumulative distribution functions are reported in
131 Supplementary Figure 2), showing that most of eruptions have an azimuth toward NE (50°, toward Astroni, Agnano, and
132 Solfatara). No specific differences between the distributions are visible. This observation is tested again with a two-sample
133 Kolmogorov-Smirnov test (see Supplementary Figure 3), confirming that the directions of dyke propagation are similar in all
134 epochs.

135 Rivalta et al. (2019) suggest that preferential directions may be induced by topographic peaks that locally modify the stress
136 field, which is mainly controlled by unloading. To investigate this empirically, we analyse the maxima of the topography
137 surrounding the caldera, retrieving the maxima in all directions in swaths with different length, hereinafter called radius.
138 Maximum radii from 1 to 9 km are tested: for each radius, the distribution of topographic maxima as a function of azimuth is
139 normalised and compared with the azimuthal distribution of past eruptions (Figure 2C). For simplicity, the present day
140 topography is adopted, even if some of the edifices (and the corresponding topographic peaks) were built during the post-
141 NYT activity. The comparison confirms the correlation anticipated by Rivalta et al. (2019). The primary peak is NE (around
142 50°) corresponds to the topographic peak associated with La Starza marine terrace (Fig. 1, for a radius of 1 km) and
143 Camaldoli Hill (for radii of 3 km and larger). In agreement with Rivalta et al. (2019), the latter topographic peak is the most
144 pronounced and it coincides with the highest concentration of eruptive vents during various eruptive periods. A secondary
145 peak appears in the NNW direction (around 330°) for intermediate radii (between 3 and 5 km), corresponding to the peak of
146 the Gauro volcanic edifice (Monte Barbaro): this edifice was created during one of the first eruptions of the first epoch, and
147 does not correspond to any peak in the observed distribution of azimuth. However, this secondary peak becomes less
148 important for large radii (7 km and above), due to the Camaldoli Hill. Performing a Kolmogorov-Smirnov test between the
149 angular distributions of past vents and of topographic peaks, the largest p-values correspond to a maximum distance of 7 km.
150 The null hypothesis of equal distribution is consistently not rejected independently from vent position uncertainty only for
151 radii of 7 and 9 km, while it is rejected for smaller radii (Supplementary Figure 4).

152



153
154
155
156
157

Figure 2: (A) Empirical distribution of distances from the centre of the caldera (dyke propagation length) for Epochs 1, 2 and 3. The red line in Epoch 3 reports a Gaussian kernel smoothing the empirical distribution. (B) Empirical distribution of azimuth (dyke direction) for Epochs 1, 2 and 3. (C) Empirical distribution of azimuth (dyke direction) for all Epochs (the red line in Epoch 3 reports a Gaussian kernel smoothing the empirical distribution) and the maxima of topographic peaks in radial swaths of variable length from the caldera centre.

158

3.2 Vent opening probability for Campi Flegrei

159
160
161
162
163
164
165
166

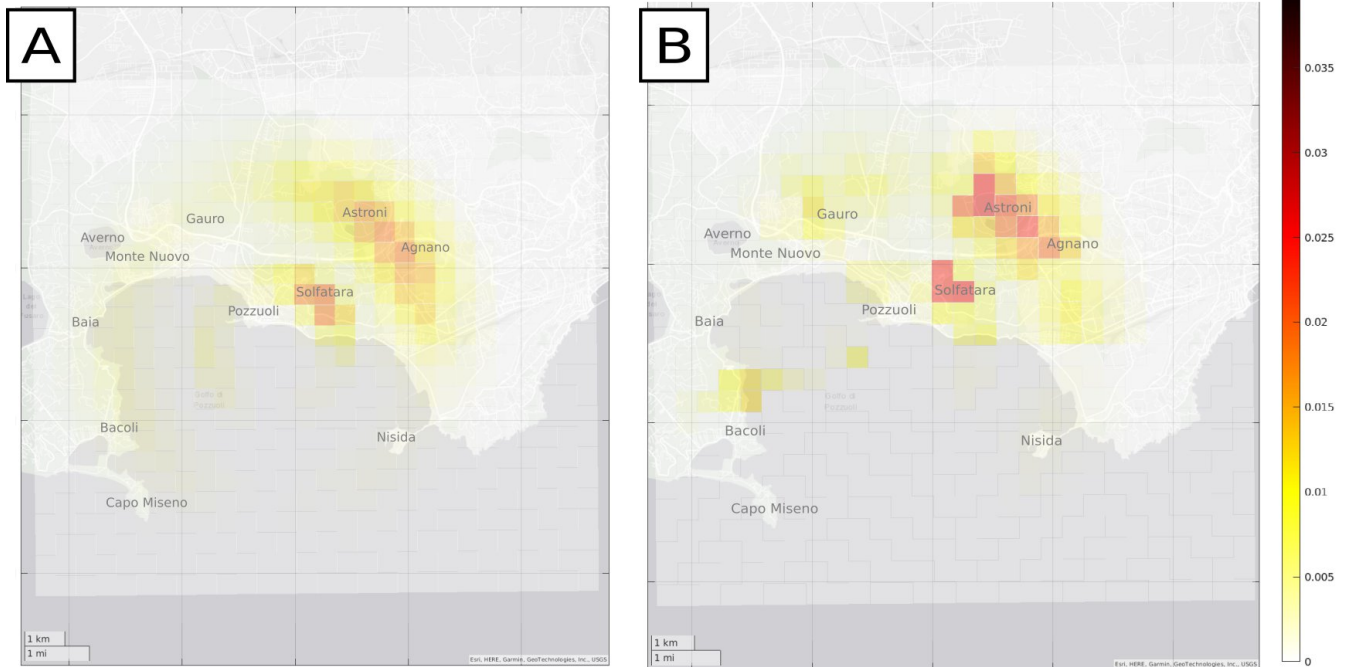
To apply Eq. (2) and quantify the vent probability map, we first test the independence of the radial and the azimuth distributions, by testing whether the direction and the distances of past vent positions are correlated to each other. To this end, we divide the directions in the 4 sectors (SW, NW, NE, and SE), and we compare the distribution of distances in the different sectors again using the Kolmogorov-Smirnov test. All the six couples are tested. The results (see Supplementary Figure 6) show that the hypothesis of equal distribution cannot be rejected for all combinations of sectors, standing for the independence of the two parameters.

To develop the probability map, we define a grid 14.5 x 12.5 km, centred at LON 427406 and LAT 4518958 (UTM WGS 84 33N), with 700 square cells 500 x 500 m, equal to the one adopted in Selva et al. (2012). Then, the probability in each cell is

167 computed by numerically integrating $f_{xy}(x,y)$ computed through Eq. (2), where the terms $f_r(r)$ and $f_\theta(\theta)$ can be set using the
 168 empirical distributions developed in Section 3.1.
 169 In particular, we propose 2 alternative implementations. At first, we consider for both $f_r(r)$ and $f_\theta(\theta)$ the empirical
 170 distributions that may be considered representatives of the present state of the caldera. Hereinafter, this first approach is
 171 referred to as model M1. To generalize the empirical distributions, we apply Gaussian kernels (red curves in Fig. 2A,C). The
 172 most appropriate bandwidth is defined using a leave-one-out technique with a Kullback-Leiber score (Connor et al. 2019). In
 173 particular, we set $f_r(r)$ as the radial distribution of the eruptions of Epoch 3 (including also Monte Nuovo), i.e. the most
 174 recent. As Epoch 1 is significantly different for the distribution of distances, its consideration would introduce a bias for
 175 forecasting future behaviours. Here, being very close in time to Epoch 1, Epoch 2 is assimilated to it, and only Epoch 3 is
 176 considered. The distribution is also truncated at 10 km, where it essentially the distribution drops to 0 (red line in Fig. 1A).
 177 The more appropriate bandwidth is found to be 275 m (Supplementary Figure 6a). To set $f_\theta(\theta)$, we instead consider the
 178 azimuth distribution of all post-NYT eruptions (red line in Fig 1C), as the different epochs are statistically indistinguishable.
 179 For the kernel, the more appropriate bandwidth is found to be 17 degrees (Supplementary Figure 6b).
 180 A second implementation is also tested by setting $f_\theta(\theta)$ differently, that is by substituting the empirical azimuth distribution
 181 adopted in M1 with the distribution of the topographic maxima for a radius of 7,000 m, the one that better correlates with
 182 past vents. Hereinafter, this second approach is referred to as model M2.
 183 The results of the two alternative implementations M1 and M2 are reported in Figure 3. The numerical values for both
 184 models are reported as Supplementary File.

M1: Empirical distributions

M2: Empirical distribution+ topographic profile



185 **Figure 3:** Vent opening probability maps: (A) model M1, based empirical distances and azimuth, (B) model M2, based on empirical
 186 distances and topographic azimuth.
 187

188

189 **4. Discussion**

190 The resulting maps are similar, with two distinct probability peaks in the NE direction at about 4 and 2 km from the centre,
191 corresponding to the Agnano-Astroni and the Solfatara area, respectively. In M2, which considers the topographic
192 contribution (Figure 3B), the angular probability values are less smoothed than in model M1, where the empirical
193 distributions are smoothed by the kernels (Figure 3A). The effect is that the maximum probability values in the area at NE is
194 almost halved in M1; also the relative peaks in the other directions appear relatively more evident in M2, with secondary
195 peaks in the submerged side of the caldera toward W, in the direction of Bacoli, as well as the inland area toward NNW. On
196 the contrary, in M1 probabilities are more distributed, generating two concentric and separated rings of larger probabilities at
197 2 and 4 km from the caldera centre.

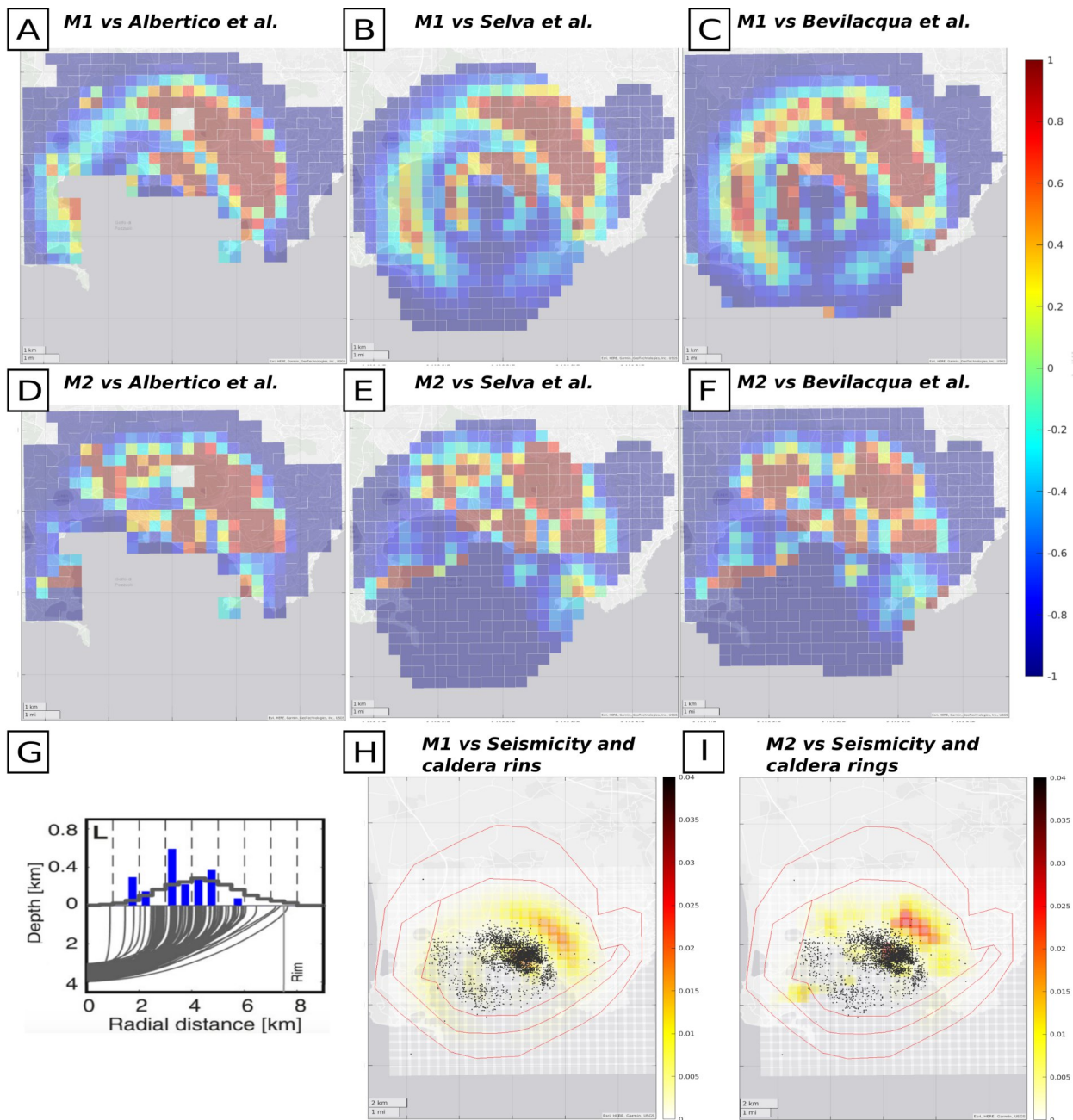
198 Comparing these results with the main probability maps for Campi Flegrei discussed in the literature - Alberico et al.
199 (2002), Selva et al. (2012), and Bevilacqua et al. (2015), hereinafter indicated as A02, S12 and B15, respectively - interesting
200 coincidences and some significant differences emerge. As already noted, the map produced by A02 differs widely from S12
201 and B15 maps, having maximum values in the centre of the caldera, which is in contrast with the empirical evidence of
202 recent past vents. In this, M1 and M2 are closer to S12 and B15, providing lower probabilities close to the caldera centre and
203 larger probabilities in the NE area of Astroni and Agnano, where most of past vents concentrate.

204 To better highlight further similarities and differences, in Figure 4A-F we report the maps of the relative differences in
205 probability between M1, M2 and A02, S12, and B15, rescaling all of them to the same grid and, for S12 and B15,
206 considering the mean of the epistemic uncertainty (Supplementary Figure 7). These maps highlight that the main differences
207 are connected to the two rings discussed above, which were not present in previous studies.

208 The outer ring, at 4 km, coincides with the area identified by Charlton et al. (2020), and includes the higher probability area
209 of S12 and B15, located in the Agnano area to the NE of the caldera. However, also in this area, both M1 and M2 provide
210 larger probabilities (panels B, C, E, F). This ring also includes the area of Monte Nuovo (N, last eruption at Campi Flegrei),
211 and especially M1 provides larger probabilities than previous studies. Also the secondary peak identified in the Averno area
212 (NW) in S12 is found in M1 and M2, but shifted inward and eastward, in the direction of Gauro. The outer ring also
213 generates several other secondary probability peaks at sea in the W directions, in the direction of the topographic peaks of
214 Baia/Bacoli, especially in M1. These peaks are larger than in literature maps. On the other hand, in the areas of Nisida (SE)
215 and Capo Miseno (SW), the probability values obtained here are relatively lower than the ones in literature.

216 The inner ring includes the high probability area of Solfatara, present in both S12 and B15, but also in this case both M1 and
217 M2 provide larger probabilities (Fig. 4B, C, E, F). In addition, the inner ring introduces new peaks in probability within the
218 bay, toward W, and in the coastal area of La Starza, toward E, both less pronounced in previous studies.

219 Also in the outer area of the caldera, external to the outer ring, M1 and M2 are different than previous studies. Here, M1 and
220 M2 do not assume that vent opening may occur only inside the caldera border, as in S12 and B15, but an outer limit is
221 established by the maximum observed distance from the centre of the caldera in Epoch 3 (Section 3.1). This cuts out the
222 most external areas, mainly toward E, NW and S, where both M1 and M2 foreseen smaller probabilities than previous
223 models.



224
 225 **Figure 4:** Relative difference between (A) M1 and Albertico et al. (2002), (B) M2 and Alberico et al. (2002), (C) M1 and Selva et al.
 226 (2012), (D) M2 and Selva et al. (2012), (E) M1 and Bevilacqua et al. (2015), (F) M2 and Bevilacqua et al. (2015). Positive numbers mean
 227 that M1/M2 are larger than literature studies. (G) Forecasted distances from the centre of the caldera from Rivalta et al. (2019).
 228 Comparison between the spatial distribution of Campi Flegrei seismicity ($M_d > 0.5$) in the period June 2023 - June 2025, the caldera rims
 229 (as mapped in Natale et al. 2024, 2025), and M1 (panel H) and M2 (panel I).
 230
 231

232 5. Conclusions

233 The vent opening maps derived in the paper are based on assumptions radically different from the ones in literature. The
234 approach is inspired from the dyke propagation model proposed in Rivalta et al. (2019), which suggests a substantial
235 independence between the radial and azimuthal distributions of dykes propagating from the centre of the caldera. The results
236 confirm some of the features already highlighted in previous studies, but also it introduces important differences. In
237 particular, the most striking difference is that the vent probability peaks in two circles at around 2 and 4 km from the caldera
238 centre, with significant modulations in the different directions, while smaller probabilities are found in the peripheral areas
239 of the caldera. These rings, particularly evident in model M1 but present also in model M2, are compatible with in the range
240 forecasted by Rivalta et al. (2019) when adopting only Epoch 3 data (Fig. 4G). However, the propagation distance
241 distribution here produces two distinct peaks at 2 and 4 km, more than a continuous distribution in this range. The inner
242 circle essentially coincides with an area characterized by high seismic activity recorded in the ongoing unrest episode (black
243 dots in Fig. 4H,I), while the outer circle is instead closer to the the position of the ring faults surrounding the inner caldera
244 (red lines in Fig. 4H-I, Natale et al. 2024, 2025). These observations are completely independent and seem to spot privileged
245 paths for magma ascent around the inner caldera border. This may be the subject of future studies.

246 It is important to stress that M1 and M2 are produced using the empirical distributions which are considered relevant for
247 forecasting future occurrences, that is Epoch 3 for distances, and either all epochs or topographic peaks for angles. Indeed,
248 while the distribution of the azimuth does not change significantly across epochs, the analysis of the distances with respect to
249 the centre of the caldera has shown that Epoch 1 differs significantly from Epoch 3 in terms of distances. This confirms the
250 findings of Rivalta et al. (2019), and it is in agreement with Orsi et al. (2004), who concluded that the last change in stress
251 regime occurred prior to onset of the Epoch 3, and suggested that only the past 5 ka should be considered as reference for the
252 present state of the caldera (Orsi et al. 2009). This assumption was adopted also in Selva et al. (2012).

253 Finally, even if here we develop two maps, we prefer not to quantify the epistemic uncertainty on the proposed approach,
254 differently from what was done in previous studies like Selva et al. (2012) and Bevilacqua et al (2015). The reason is that
255 several case studies recently demonstrated that the effective epistemic uncertainty on a target physical process (here vent
256 opening) is better estimated by combining radically alternative approaches (e.g., defining weighted ensembles of alternative
257 models), rather than by exploring the epistemic uncertainty inherent to one specific approach (Selva et al. 2015; Marzocchi
258 et al. 2021; Meletti et al. 2021, among the others). Consequently, while the epistemic uncertainty on a given approach may
259 be of relative interest, the very development of an alternative approach like the one presented here may be a significant
260 added value to future quantification of epistemic uncertainty in the process of vent opening at Campi Flegrei, via multi-
261 model ensembles or equivalent approaches that combine all the scientifically grounded approaches available in literature
262 (e.g. SSHAC 1997, Marzocchi et al. 2017, 2021).

263 Datasets

264 The position of the vents related to past eruptions was obtained from Bevilacqua et al. (2015). The DEM used to find
265 topographic peaks around Campi Flegrei is TINITALY (Tarquini et al. 2023) with WGS 84 / UTM zone 33N coordinates,
266 available at <https://tinitaly.pi.ingv.it/>.

267 Author contributions

268 JS and NM conceived and developed the Methodology. JS supervised the project. NM implemented the preliminary software
270 for the analyses, with the support of JS. JS finalized the software and prepared the original draft. All the authors reviewed
271 and approved the manuscript.

272 Acknowledgments

273 The figures and maps have been produced using Matlab and/or InkScape software.

- 277 Alberico, I., Lirer, L., Petrosino, P., & Scandone, R. (2002). A methodology for the evaluation of long-term volcanic risk
278 from pyroclastic flows in Campi Flegrei (Italy). *Journal of Volcanology and Geothermal Research*, 116, 63–78.
279 [https://doi.org/10.1016/S0377-0273\(02\)00211-1](https://doi.org/10.1016/S0377-0273(02)00211-1)
280
- 281 Amoruso, A., Crescentini, L., Sabetta, I., De Martino, P., Obrizzo, F., & Tammaro, U. (2014). Clues to the cause of the
282 2011–2013 Campi Flegrei caldera unrest, Italy, from continuous GPS data. *Geophysical Research Letters*, 41, 1–7.
283 <https://doi.org/10.1002/2014GL059539>
284
- 285 Barberi, F., Corrado, G., Innocenti, F., & Luongo, G. (1984). Phlegraean fields 1982–1984: Brief chronicle of a volcano
286 emergency in a densely populated area. *Bulletin of Volcanology*, 47, 175–185. <https://doi.org/10.1007/BF01961547>
287
- 288 Bevilacqua, A., Isaia, R., Neri, A., Vitale, S., Aspinali, W. P., Bisson, M., Flandoli, F., Baxter, P. J., Bertagnini, A., Ongaro,
289 T. E., Iannuzzi, E., Pistolesi, M., & Rosi, M. (2015). Quantifying volcanic hazard at Campi Flegrei caldera (Italy) with
290 uncertainty assessment: 1. Vent opening maps. *Journal of Geophysical Research: Solid Earth*, 120, 2309–2329.
291 <https://doi.org/10.1002/2014JB011775>
292
- 293 Bevilacqua A, Flandoli F, Neri A, Isaia R, Vitale S (2016). Temporal models for the episodic volcanism of Campi Flegrei
294 caldera (Italy) with uncertainty quantification. *J Geophys Res Solid Earth* 121:7821–7845.
295 <https://doi.org/10.1002/2016JB013171>
296
- 297 Bevilacqua, A., Neri, A., De Martino, P. et al. (2024) Accelerating upper crustal deformation and seismicity of Campi
298 Flegrei caldera (Italy), during the 2000–2023 unrest. *Commun Earth Environ* 5, 742.
299 <https://doi.org/10.1038/s43247-024-01865-y>
300
- 301 Bevilacqua, A., Neri, A., De Martino, P. et al. (2024). Accelerating upper crustal deformation and seismicity of Campi
302 Flegrei caldera (Italy), during the 2000–2023 unrest. *Commun Earth Environ* 5, 742. [https://doi.org/10.1038/s43247-024-](https://doi.org/10.1038/s43247-024-01865-y)
303 [01865-y](https://doi.org/10.1038/s43247-024-01865-y)
304
- 305 Bonferroni C., 1936. Teoria statistica delle classi e calcolo delle probabilità. *Pubblicazioni del Regio Istituto Superiore di*
306 *Scienze Economiche e Commerciali di Firenze*, 8, 3–62. (in Italian).
307
- 308 Buono, G., Paonita, A., Pappalardo, L., Caliro, S., Tramelli, A., & Chiodini, G. (2022). New insights into the recent magma
309 dynamics under Campi Flegrei caldera (Italy) from petrological and geochemical evidence. *Journal of Geophysical*
310 *Research: Solid Earth*, 127, e2021JB023773. <https://doi.org/10.1029/2021JB023773>
311
- 312 Buono, G., Maccaferri, F., Pappalardo, L., Tramelli, A., Caliro, S., Chiodini, S., Pinel, V., Rivalta, E., Spagnuolo, E.,
313 Trasatti, E., Di Vito, M.A. (2025). Weak Crust Owing Past Magmatic Intrusions Beneath Campi Flegrei Identified: The
314 Engine for Bradyseismic Movements? *AGU Advances*, 6, e2024AV001611. <https://doi.org/10.1029/2024AV001611>
315
- 316 Charlton, D., Kilburn, C., & Edwards, S. (2020). Volcanic unrest scenarios and impact assessment at Campi Flegrei caldera,
317 Southern Italy. *Journal of Applied Volcanology*, 9(7). <https://doi.org/10.1186/s13617-020-00097-x>
318
- 319 Chiodini, G., et al. (2021). Hydrothermal pressure–temperature control on CO₂ emissions and seismicity at Campi Flegrei
320 (Italy). *Journal of Volcanology and Geothermal Research*, 414, 107245. <https://doi.org/10.1016/j.jvolgeores.2021.107245>
321
- 322 D’Antonio, M., Tonarini, S., Arienzo, I., Civetta, L., & Di Renzo, V. (2007). Components and processes in the magma
323 genesis of the Phlegraean Volcanic District (Southern Italy). In L. Beccaluva, G. Bianchini, & M. Wilson (Eds.), *Cenozoic*
324 *volcanism in the Mediterranean area* (pp. 203–220). Geological Society of America Special Paper 418.

325
326 Del Gaudio, C., Aquino, I., Ricciardi, G. P., Ricco, C., & Scandone, R. (2010). Unrest episodes at Campi Flegrei: A
327 reconstruction of vertical ground movements during 1905–2009. *Journal of Volcanology and Geothermal Research*, 195,
328 48–56. <https://doi.org/10.1016/j.jvolgeores.2010.02.002>
329
330 Di Vito, M. A., Acocella, V., Aiello, G., Barra, D., Battaglia, M., Carandente, A., Del Gaudio, C., De Vita, S., Ricciardi, G.
331 P., Ricco, C., Scandone, R., & Terrasi, F. (2016). Magma transfer at Campi Flegrei caldera (Italy) before the 1538 AD
332 eruption. *Scientific Reports*, 6, 32245. <https://doi.org/10.1038/srep32245>
333
334 Di Vito, M. A., Isaia, R., Orsi, G., Southon, J., de Vita, S., D'Antonio, M., Pappalardo, L., & Piochi, M. (1999). Volcanism
335 and deformation since 12,000 years at the Campi Flegrei caldera (Italy). *Journal of Volcanology and Geothermal Research*,
336 91(2–4), 221–246. [https://doi.org/10.1016/S0377-0273\(99\)00037-2](https://doi.org/10.1016/S0377-0273(99)00037-2)
337
338 Fernandez, G., Giaccio, B., Costa, A., Monaco, L., Nomade, S., Albert, P. G., Pereira, A., Flynn, M., Leicher, N., Lucchi, F.,
339 Petrosino, P., Palladino, D. M., Milia, A., Insinga, D. D., Wulf, S., Kearney, R., Veres, D., Jordanova, D., Putignano, M. L.,
340 Isaia, R., & Sottili, G. (2024). New constraints on the Middle–Late Pleistocene Campi Flegrei explosive activity and
341 Mediterranean tephrostratigraphy (~160 ka and 110–90 ka). *Quaternary Science Reviews*, 331, Article 108623.
342 <https://doi.org/10.1016/j.quascirev.2024.108623>
343
344 Gibbons, J. D., and S. Chakraborti (2003), *Non-parametric Statistical Inference*, 4th ed., 645 pp., Marcel Dekker, New York
345
346 Giudicepietro, F., Avino, R., Bellucci Sessa, E., et al. (2025). Burst-like swarms in the Campi Flegrei caldera accelerating
347 unrest from 2021 to 2024. *Nature Communications*, 16, 1548. <https://doi.org/10.1038/s41467-025-56723-y>
348
349 Isaia, R., Marianelli, P., & Sbrana, A. (2009). Caldera unrest prior to intense volcanism in Campi Flegrei (Italy) at 4.0 ka
350 B.P.: Implications for caldera dynamics and future eruptive scenarios. *Geophysical Research Letters*, 36, L06304.
351 <https://doi.org/10.1029/2008GL036962>
352
353 Isaia, R., Vitale, S., Marturano, A., Aiello, G., Barra, D., Ciarcia, S., Iannuzzi, E., & Tramparulo, F. D'A. (2019).
354 High-resolution geological investigations to reconstruct the long-term ground movements in the last 15 kyr at Campi Flegrei
355 caldera (southern Italy). *Journal of Volcanology and Geothermal Research*. Advance online publication.
356 <https://doi.org/10.1016/j.jvolgeores.2019.07.012>
357
358 Monaco, L., Palladino, D. M., Albert, P. G., Arienzo, I., Conticelli, S., Di Vito, M., Fabbrizio, A., D'Antonio, M., Isaia, R.,
359 Manning, C. J., Nomade, S., Pereira, A., Petrosino, P., Sottili, G., Sulpizio, R., Zanchetta, G., & Giaccio, B. (2022). Linking
360 the Mediterranean MIS 5 tephra markers to Campi Flegrei (southern Italy) 109–92 ka explosive activity and refining the
361 chronology of MIS 5c-d millennial-scale climate variability. *Global and Planetary Change*, 211, Article 103785.
362 <https://doi.org/10.1016/j.gloplacha.2022.103785>
363
364 Natale, J., Ferranti, L., Isaia, R., Marino, C., Sacchi, M., Spiess, V., Steinmann, L., & Vitale, S. (2022). Integrated
365 on-land-offshore stratigraphy of the Campi Flegrei caldera: New insights into the volcano-tectonic evolution in the last
366 15 kyr. *Basin Research*, 34(2), 855–882. <https://doi.org/10.1111/bre.12643>
367
368 Natale, J., Vitale, S., Repola, L., Monti, L., and Isaia, R. (2024); Geomorphic analysis of digital elevation model generated
369 from vintage aerial photographs: A glance at the pre-urbanization morphology of the active Campi Flegrei caldera.
370 *Geomorphology* 460, 109267; <https://doi.org/10.1016/j.geomorph.2024.109267>
371
372 Natale, J., Cascella, E., & Vitale, S. (2025); Tracking the growth and deformation of fissure phreatomagmatic eruptions:
373 Insights from the ca. 3.9 ka Nisida eruption at Campi Flegrei caldera, southern Italy. *GSA Bulletin* 2025; doi:
374 <https://doi.org/10.1130/B38367.1>

375 Orsi, G., Di Vito, M. A., & Isaia, R. (2004). Volcanic hazard assessment at the restless Campi Flegrei caldera. *Bulletin of*
376 *Volcanology*, 66, 514–530. <https://doi.org/10.1007/s00445-003-0327-4>
377
378 Osservatorio Vesuviano (2025), Bollettino di Sorveglianza CAMPI FLEGREI GIUGNO 2025 A cura della Sezione di
379 Napoli, available at [https://www.ov.ingv.it/index.php/monitoraggio-e-infrastrutture/bollettini-tutti/bollett-mensili-cf/anno-](https://www.ov.ingv.it/index.php/monitoraggio-e-infrastrutture/bollettini-tutti/bollett-mensili-cf/anno-2025-3/1850-bollettino-mensile-campi-flegrei-2025-06/file)
380 [2025-3/1850-bollettino-mensile-campi-flegrei-2025-06/file](https://www.ov.ingv.it/index.php/monitoraggio-e-infrastrutture/bollettini-tutti/bollett-mensili-cf/anno-2025-3/1850-bollettino-mensile-campi-flegrei-2025-06/file)
381 Pappalardo, L., Civetta, L., D'Antonio, M., Deino, A. L., Di Vito, M. A., Orsi, G., Caradente, A., De Vita, S., Isaia, R., &
382 Piochi, M. (1999). Chemical and Sr-isotopical evolution of the Phlegraean magmatic system before the Campanian
383 Ignimbrite (37 ka) and the Neapolitan Yellow Tuff (12 ka) eruptions. *Journal of Volcanology and Geothermal Research*,
384 *91*(1), 141–166.
385
386 Rivalta, E., Corbi, F., Passarelli, L., Acocella, V., Davis, T., & Di Vito, M. A. (2019). Stress inversions to forecast magma
387 pathways and eruptive vent location. *Science Advances*, 5, eaau9784. <https://doi.org/10.1126/sciadv.aau9784>
388
389 Scarpati, C., Perrotta, A., Lepore, S., & Calvert, A. (2013). Eruptive history of Neapolitan volcanoes: Constraints from
390 $^{40}\text{Ar}/^{39}\text{Ar}$ dating. *Geological Magazine*, 150(3), 412–425. <https://doi.org/10.1017/S0016756812000731>
391
392 Selva, J., Orsi, G., Di Vito, M. A., Marzocchi, W., & Sandri, L. (2012). Probability hazard map for future vent opening at the
393 Campi Flegrei caldera, Italy. *Bulletin of Volcanology*, 74, 497–510. <https://doi.org/10.1007/s00445-011-0528-2>
394
395 Smith, V. C., Isaia, R., & Pearce, N. J. G. (2011). Tephrostratigraphy and glass compositions of post–15 kyr Campi Flegrei
396 eruptions: Implications for eruption history and chronostratigraphic markers. *Quaternary Science Reviews*, 30, 3638–3660.
397 <https://doi.org/10.1016/j.quascirev.2011.08.017>
398
399 Sparice, D., Pelullo, C., de Vita, S., Arienzo, I., Petrosino, P., Mormone, A., Di Vincenzo, G., Marfè, B., Cariddi, B., De
400 Lucia, M., Vertechi, E., D’Oriano, C., Del Carlo, P., Di Roberto, A., Giaccio, B., Zanchetta, G., & Di Vito, M. A. (2024).
401 The pre-Campi Flegrei caldera (>40 ka) explosive volcanic record in the Neapolitan Volcanic Area: New insights from a
402 scientific drilling north of Naples. *Journal of Volcanology and Geothermal Research*.
403 <https://doi.org/10.1016/j.jvolgeores.2024.108209>
404
405 Tarquini, S., Isola, I., Favalli, M., Battistini, A., & Dotta, G. (2023). TINITALY, a digital elevation model of Italy with a
406 10 m cell size (Version 1.1) [Data set]. Istituto Nazionale di Geofisica e Vulcanologia (INGV).
407 <https://doi.org/10.13127/tinality/1.1>
408
409 Vitale, S., & Natale, J. (2023). Combined volcano-tectonic processes for the drowning of the Roman western coastal
410 settlements at Campi Flegrei (southern Italy). *Earth, Planets and Space*, 75, 38. <https://doi.org/10.1186/s40623-023-01795-7>